HHS Public Access

Author manuscript

Nature. Author manuscript; available in PMC 2013 March 13.

Published in final edited form as:

Nature. 2012 September 13; 489(7415): 322–325. doi:10.1038/nature11317.

hESC-Derived Cardiomyocytes Electrically Couple and Suppress Arrhythmias in Injured Hearts

Yuji Shiba[1,4,*], **Sarah Fernandes**[1,*], **Wei-Zhong Zhu**[1], **Dominic Filice**[1,2], **Veronica Muskheli**[1], **Jonathan Kim**[1], **Nathan J. Palpant**[1], **Jay Gantz**[1,2], **Kara White Moyes**[1], **Hans Reinecke**[1], **Benjamin Van Biber**[1], **Todd Dardas**[3], **John L. Mignone**[3], **Atsushi Izawa**[4], **Ramy Hanna**[3], **Mohan Viswanathan**[3], **Joseph D. Gold**[5], **Michael I. Kotlikoff**[6], **Narine Sarvazyan**[7], **Matthew W. Kay**[7,8], **Charles E. Murry**[1,2,3], and **Michael A. Laflamme**[1]

[1]Department of Pathology, Center for Cardiovascular Biology, Institute for Stem Cell and Regenerative Medicine, University of Washington, Seattle, WA

[2]Department of Bioengineering, Center for Cardiovascular Biology, Institute for Stem Cell and Regenerative Medicine, University of Washington, Seattle, WA

[3]Department of Medicine/Cardiology, Center for Cardiovascular Biology, Institute for Stem Cell and Regenerative Medicine, University of Washington, Seattle, WA

[4]Department of Cardiovascular Medicine, Shinshu University, Matsumoto, Japan

[5]Geron Corporation, Menlo Park, CA

[6]Department of Biomedical Sciences, College of Veterinary Medicine, Cornell University, Ithaca, NY

[7]Department of Pharmacology & Physiology, The George Washington University, Washington, DC

[8]Department of Electrical & Computer Engineering, The George Washington University, Washington, DC

Abstract

Transplantation studies in mice and rats have shown that human embryonic stem cell-derived cardiomyocytes (hESC-CMs) can improve the function of infarcted hearts[1–3], but two critical

Address correspondence to: Michael A. Laflamme, 850 Republican St., Seattle, WA 98109, USA. Phone: 206.897.1518; Fax: 206.897.1540; laflamme@u.washington.edu. Or to: Charles E. Murry, 850 Republican St., Seattle, WA 98109, USA. Phone: 206.616.8685; Fax: 206.897.1540; murry@uw.edu.

*These authors contributed equally to this study.

Author Contributions

SF, YS, WZZ, DF, MIK, JDG, CEM and MAL designed the study. YS and SF led the arrhythmia and calcium imaging experiments, respectively. YS developed and performed the telemetry and programmed electrical stimulation. TD, JLM, AI, RH and MV performed telemetric ECG interpretation. The GCaMP3+ hESC line was generated by JG, NJP, and BVB. VM, JK, KWM, SF and YS performed and analyzed immunohistochemistry. SF, HR and MAL developed and performed guinea pig-specific in situ hybridization. SF, WZZ and DF performed and analyzed the GCaMP3 imaging experiments. DF, MWK and NS developed and analyzed the voltage mapping experiments. All authors contributed to data analysis and interpretation. YS made the figures with assistance of SF, WZZ, KWM and DF. CM and MAL wrote the manuscript.

issues related to their electrophysiological behavior in vivo remain unresolved. First, the risk of arrhythmias following hESC-CM transplantation in injured hearts has not been determined. Second, the electromechanical integration of hESC-CMs in injured hearts has not been demonstrated, so it is unclear if these cells improve contractile function directly through addition of new force-generating units. Here we use a guinea pig model to show hESC-CM grafts in injured hearts protect against arrhythmias and can contract synchronously with host muscle. Injured hearts with hESC-CM grafts show improved mechanical function and a significantly reduced incidence of both spontaneous and induced ventricular tachycardia (VT). To assess the activity of hESC-CM grafts in vivo, we transplanted hESC-CMs expressing the genetically-encoded calcium sensor, GCaMP3[4, 5]. By correlating the GCaMP3 fluorescent signal with the host ECG, we found that grafts in uninjured hearts have consistent 1:1 host-graft coupling. Grafts in injured hearts are more heterogeneous and typically include both coupled and uncoupled regions. Thus, human myocardial grafts meet physiological criteria for true heart regeneration, providing support for the continued development of hESC-based cardiac therapies for both mechanical and electrical repair.

While hESC-CMs form gap junctions and beat synchronously in vitro[6, 7], there is only indirect evidence for their electromechanical integration after transplantation[6–8]. We do not know whether hESC-CM grafts contract synchronously at physiological human rates, integrate in injured hearts despite scar tissue, or affect electrical stability. Indeed, both pro-[9] and anti-[10] arrhythmic effects have been reported for mouse cardiomyocyte grafts in injured mouse hearts. Human cardiac grafts could plausibly contribute to arrhythmogenesis through automaticity[11–14] and triggered activity[15], and their irregular graft geometry could promote reentry[1–3, 16].

To address these uncertainties, we employed a novel guinea pig model of cardiac injury. Prior work with hESC-CMs in infarcted hearts was done in mice and rats[1–3], but these species' rapid heart rates (~600 and 400 beats per minute (bpm), respectively[17]) may prevent host-graft coupling or arrhythmias that could occur in humans. In vitro hESC-CMs show a spontaneous rate of ~50–150 bpm[12, 13, 18] and can be paced up to 240 bpm, suggesting they can keep up with the guinea pig heart (~200–250 bpm[19]).

We first examined the structural, mechanical and electrocardiographic consequences of hESC-CM transplantation in injured hearts of immunosuppressed guinea pigs (Supplementary Fig. S1a). hESC-CMs were derived from H7 hESCs as previously described[2, 20]. Adult guinea pigs were subjected to cardiac cryoinjury and implanted with telemetric electrocardiographic (ECG) transmitters. Ten days later, they underwent a repeat thoracotomy and intra-cardiac injection of either 1×10^8 hESC-CMs in a pro-survival cocktail (PSC) of factors previously shown to enhance hESC-CM engraftment[2] (n=15), 1×10^8 non-cardiac hESC-derivatives in PSC (Non-CMs; n=13), or PSC vehicle alone (n=14). hESC-CMs were 63% pure by anti-α-actinin flow cytometry, while non-CMs included no detectable cardiomyocytes (Supplementary Fig. S2).

At 28-days post-transplantation, all animals showed transmural scar and thinning of the left ventricle (LV). Scar area was not different amongst the groups (13.2±0.9% of the LV in hESC-CM, 14.8±1.4% in non-CM, and 15.3±1.9% in PSC-only recipients). However,

hESC-CM recipients showed partial remuscularization with islands of human myocardium occupying 8.4 ± 1.5% of the scar area (Fig. 1a). The human origin of these grafts was confirmed by in situ hybridization with a human pan-centromeric probe, and >99% of the human cells immunostained positively with the cardiac marker β-myosin heavy chain (βMHC) (Fig. 1b & Supplementary Fig. S3a–f). No teratomas developed, and hESC-CM grafts were negative for multiple non-cardiac markers (Supplementary Fig. S3g–k). Most of the graft myocardium was located in central scar, but there were occasional points of host-graft contact in the border zone with shared intercalated discs identified by anti-connexin-43 and cadherin immunostaining (Fig. 1c–h & Supplementary Fig. S3d–e). Minimal immune reaction was observed in sections stained with a guinea pig-specific pan-leukocyte marker (Supplementary Fig. S3l). Grafts were supplied by host-derived neovessels that contained erythrocytes, indicating perfusion by the host coronary circulation (Supplementary Fig. S3h,m–o).

Surviving human cells were found in only 7 of 13 non-CM recipients at 28-days post-transplantation, and these grafts were smaller than those in hESC-CM recipients (<1% of the scar area). No βMHC positive graft was detected in non-CM recipients; instead, the surviving human cells consisted of small epithelial nests and scattered fibroblastic cells (Supplementary Fig. S4).

Hearts receiving hESC-CMs, non-CMs and PSC-only were assessed by echocardiography on days −2 and +28 relative to cell transplantation. All groups showed increased LV dimensions and reduced fractional shortening (FS) on day −2 relative to uninjured controls (n=11), but there were no differences among the cryoinjured groups (Fig. 1i & Supplementary Fig. S5). The two control groups exhibited further LV dilation and deterioration of FS between days −2 and +28 ($p<0.05$ for all pairwise comparisons between time-points). This deterioration was completely attenuated in cryoinjured hESC-CM recipients, who showed significantly greater FS on day +28 than PSC-only or non-CM controls ($p<0.05$ and $p<0.01$, respectively) (Fig. 1i).

Ambulatory telemetric ECG recordings were obtained regularly from 1 day post-injury to 28 days post-transplantation. Pilot studies revealed only rare premature ventricular contractions (PVCs) in uninjured animals, while cryoinjured but not transplanted animals showed occasional PVCs and runs of ventricular tachycardia (VT) (Supplementary Table S1). Interestingly, the hESC-CM group had the lowest fraction of animals with PVCs after transplantation and the lowest rate of couplet PVCs per hour (Supplementary Fig. S6). Moreover, fewer hESC-CM recipients showed spontaneous VT, and hESC-CM recipients were the only group with no sustained VT (Fig. 1j–k). Next, we counted all episodes of VT from days 3–28 and found that non-CM recipients showed 785% more VT episodes than hESC-CM recipients (95% CI: 74% to +4370%, $p<0.01$; Fib 1I).

As a final test of electrical stability, we induced arrhythmias through programmed electrical stimulation (PES). To detect either a positive or negative effect of cell transplantation, we developed a PES protocol that induced VT in 40% of non-transplanted animals at 38 days post-cryoinjury (n=5), but not in uninjured animals (n= 8). When cryoinjured hESC-CM recipients were challenged with PES at 28 days post-transplantation, VT was induced in

only 6.7% of these animals versus 61.5% and 50% of cryoinjured non-CM and PSC-only recipients, respectively ($p<0.01$ by Fisher's exact test, Fig. 1m–n).

To explore the mechanism by which hESC-CMs improved mechanical and electrical function, we investigated whether the grafts were coupled and beat synchronously with host myocardium. We used zinc-finger nuclease (ZFN) mediated transgenesis[21] to create hESC-CMs that stably expressed the genetically encoded fluorescent calcium sensor, GCaMP3[4, 5], and these myocytes exhibited robust fluorescence transients with each contractile cycle in vitro (Supplementary Fig. S7 & Movie S1). We transplanted 1×10^8 GCaMP3+ hESC-CMs (cardiac purity of 74±10%) into intact and cryoinjured guinea pig hearts and performed intravital imaging at 2- or 4-weeks post-transplantation (Supplementary Fig. S1b). Epicardial fluorescent transients indicated activation of the graft in vivo, and these were correlated with the ECG to determine their synchrony with host myocardium[10].

The GCaMP3+ hESC-CM grafts in uninjured hearts had extensive host-graft contact with little intervening fibrosis (Fig. 2a & Supplementary Fig. S8a). Correspondingly, these hearts showed an impressive degree of host-graft electromechanical integration. We found large GCaMP3+ hESC-CMs grafts in all uninjured recipients at 14 days post-transplantation (n=9), and 100% of the visible graft in each animal calcium fluorescence transients that synchronized 1:1 with systole in the host ECG (Fig. 2b). These hearts were also imaged ex vivo during mechanical arrest with either 2,3-butanedione monoxime (BDM) or blebbistatin (n=11). 1:1 host-graft coupling continued under these conditions, ruling out confounding motion artifacts and the possibility of indirect graft activation by passive stretch (Supplementary Fig. S8 b–c & Movie S2). hESC-CM grafts in uninjured hearts remained fully coupled during pacing at rates ≥5Hz (Fig. 2c).

Next, we transplanted GCaMP3+ hESC-CMs at 10 days post-cryoinjury and performed intravital imaging at 14 and 28 days post-transplantation (n=7 and n=15 animals, respectively). By histology, surviving grafts at both timepoints were mostly located within the central scar, although occasional points of host-graft contact in the border zone were identified (Fig. 3a & Supplementary Fig. S9a). Dual-labeling with a guinea pig-specific in situ probe and anti-GFP immunostaining ruled out a significant contribution of cell fusion to the observed GCaMP3 signals (Supplementary Fig. S9b & Movie S3). Cryoinjured hearts with GCaMP3+ hESC-CM grafts showed robust epicardial fluorescence transients, but their behavior was more heterogeneous than that of grafts in uninjured animals, with greater variation in size, distribution and temporal relationship to the host ECG.

Given this complicated behavior, we focused on imaging mechanically arrested hearts ex vivo, where the grafts could be more completely visualized and the proportion of coupled and uncoupled graft better quantified (Supplementary Movies S4–S5). We found regions of GCaMP3+ graft with consistent 1:1 host-graft coupling in ~60% of hearts at both 14- and 28-days post-transplantation (4 of 7 and 9 of 15 animals, respectively; Fig. 3b & Supplementary Tables S2–S3). While there was no significant difference in the fraction of animals with coupled graft between the two timepoints, in the subset of animals with at least some coupling, there was a trend toward greater host-graft coupling over time (66±10% versus 87±6% of visible graft at 14 and 28 days, respectively). No grafts with intermittent or

partial coupling (e.g. 1:2 or 1:3 host-graft coupling) were observed. Uncoupled graft regions showed regular GCaMP3 fluorescent transients, but these occurred with a periodicity unrelated to the ECG or neighboring graft domains, usually at a rate slower than the host (at 28-days, 96±11 bpm versus a host rate of 176±9 bpm). By marking the coupled and non-coupled graft regions with indelible inks that survive histological processing, we found numerous examples of reliably coupled graft located within the central scar region, proving that coupling is not limited to grafts at the border zone (data not shown). When injured hearts with GCaMP3+ hESC-CM grafts were paced, most of the initially coupled graft regions remained coupled up to 4 Hz, after which some loss of coupling was observed (Supplementary Fig. S10).

We next attempted to perform voltage mapping of graft and host myocardium in cryoinjured hearts, but, surprisingly, hESC-CM grafts failed to label with the potentiometric dyes RH237 and di-4-ANEPPS (Supplementary Fig. S11). hESC-CMs labeled in vitro (Supplementary Fig. S12), so their poor staining in vivo likely reflects sluggish perfusion of the graft tissue and perhaps reduced membrane staining because of undeveloped T-tubules[22]. However, we did obtain excellent labeling of host myocardium with RH237 and so compared voltage maps from cryoinjured hearts with and without grafts (n=6 and n=4 animals, respectively). As expected, both groups showed robust propagation in uninjured myocardium, while optical action potential amplitudes and epicardial conduction velocities were reduced in the cryoinjury zone. The two groups showed no significant differences in the amplitudes of optical action potentials within the injured zone or the kinetics of activation and repolarization (Supplementary Figs. S13–14), suggesting that hESC-CM transplantation does not exert major paracrine effects on host electrical behavior.

Because the electrical activity of hESC-CM grafts could not be evaluated with potentiometric dyes, we instead used the GCaMP3 signal to assess graft activation and propagation. GCaMP3 transients lag depolarization due to slow binding of calcium, but this delay should be the same throughout the graft[10, 23], so graft activation maps can be generated using the time interval between electrical stimulation (or host QRS) and the GCaMP3 transient. This revealed a striking difference in activation between grafts located in viable host muscle versus those in scar tissue (Fig. 3c–d). Grafts in intact myocardium were activated uniformly and within ~10 ms, likely reflecting synchronous activation via multiple points of contact with the host. In contrast, graft activation within scar tissue was spatially and temporally heterogeneous, even in regions with 1:1 coupling. These coupled grafts showed initial activation within ~10–20 ms, but the spread of activation was slower, such that some areas required >50 ms for activation. This likely reflects the more limited contacts between graft and host, as well as slower propagation within the immature graft myocardium.

These intravital imaging studies represent the first direct demonstration that human cardiomyocytes can integrate and contract synchronously with host myocardium. While additional paracrine mechanisms cannot be excluded, the demonstration of electromechanically coupled grafts in injured hearts supports the hypothesis that hESC-CMs can improve mechanical function by creating new force-generating units, a sine qua non for heart regeneration. However, hESC-CM grafts in injured hearts were not always fully

integrated, implying that enhancing their integration may further benefit contractile function. The model developed here represents a reasonably high-throughput platform to test strategies to improve host-graft integration (e.g. tissue engineering, attenuating graft cell death and reducing fibrosis).

Our study also provides reassurance about the arrhythmogenic risk of cardiac repair with immature stem cell-derived cardiomyocytes. Consistent with prior transplantation studies by Roell et al with primary fetal mouse cardiomyocytes[10], we observed an arrhythmia-suppressive effect that was unique to cardiomyocyte grafts and occurred despite incomplete host-graft coupling. While encouraging, prior to clinical translation of hESC-based therapies, it will be essential to perform safety and efficacy studies with longer duration of follow-up and in a large animal model.

Full Methods

Cell preparation

Undifferentiated H7 hESCs[24] were expanded using either mouse embryonic fibroblast-conditioned medium (MEF-CM)[25] or a defined medium supplemented with basic fibroblast growth factor and transforming growth factor-β1 (R&D Systems)[26]. hESCs were then differentiated into cardiomyocytes using our previously reported directed differentiation protocol that involves the serial application of activin A and bone morphogenetic protein-4 (BMP4, R&D) under defined, serum-free, monolayer culture conditions[2, 13, 20]. Non-cardiac control cells were generated by subjecting hESCs to the same protocol but without the addition of activin A and BMP4. See Supplementary Fig. S2 for additional immunophenotypic information regarding the two cell preparations employed.

Human ESC-CMs and non-cardiac hESC derivatives were harvested and cryopreserved after 16–18 days under differentiating conditions. One day prior to harvest, cells were subjected to a pro-survival protocol, previously shown to enhance engraftment post-transplantation[2]. In brief, cultures were heat-shocked with a 30-minute exposure to 43 °C medium, followed by RPMI-B27 medium supplemented with IGF-1 (100 ng/ml, Peprotech) and cyclosporine A (0.2 μM, Sandimmune, Novartis). One day later, cultures were harvested with 0.25% trypsin/0.5 mM EDTA (Invitrogen) and cryopreserved as previously described[27].

Immediately prior to transplantation, cells were thawed at 37°C, washed with RPMI, and suspended in a 150 μl-volume per animal of pro-survival cocktail (PSC)[2], which consisted of 50% (v/v) growth factor–reduced Matrigel, supplemented with ZVAD (100 mM, benzyloxycarbonyl-Val-Ala-Asp(O-methyl)-fluoromethyl ketone, Calbiochem), Bcl-XL BH4 (cell-permeant TAT peptide, 50 nM, Calbiochem), cyclosporine A (200 nM, Wako), IGF-1 (100 ng/ml, Peprotech) and pinacidil (50 mM, Sigma).

Surgical procedures

For cardiac cryoinjury and ECG transmitter placement, male guinea pigs (650–750 g, Charles River) were anesthetized with an intraperitoneal injection of 50 mg/kg ketamine and 2 mg/kg xylazine. The skin was shaved and sterilized, a small incision was made in the right flank, and the transmitter (PhysioTel model CA-F40, DSI) was inserted in a subcutaneous

pocket. The positive and negative leads were then tunneled subcutaneously to the left fifth intercostal space and the upper sternal midline, respectively. The animal was then intubated, mechanically ventilated and anesthetized with 1.5% isoflurane. The heart was exposed by a left thoracotomy, the pericardium was opened, and a 10 mm-diameter aluminum cryoprobe, pre-cooled with liquid nitrogen, was applied to the left ventricular free wall four times for 30 seconds each. At the conclusion of the surgery, all animals received 0.025% (v/v) topical bupivicaine at the wound site, as well as 0.05 mg/kg intraperitoneal buprenorphine for analgesia.

From day −2 to day +28 relative to cell transplantation, animals were treated with an immunosuppressive regimen of methylprednisolone (2 mg/kg/day intraperitoneal) and cyclosporine A (15 mg/kg/day subcutaneous for 7 days, thereafter reduced to 7.5 mg/kg/day). The trough level of blood cyclosporine was measured on day +28 at 838±64 μg/L. Cell transplantation was performed via a repeat thoracotomy and injecting the total bolus of cells into three separate injection sites, i.e. the central cryolesion and the flanking lateral border zones.

Echocardiography

On days −2 and +28 relative to cell transplantation, animals were lightly anesthetized with inhaled 1.5% isoflurane, and then their left ventricular end-diastolic dimension (LVEDD), left ventricular end-systolic dimension (LVESD) and heart rate were measured by transthoracic echocardiography (GE Vivid 7) with a 10 MHz pediatric transducer. Fractional shortening was calculated by this equation: FS =100 × ((LVEDD−LVESD)/LVEDD). All echocardiographic scans and analyses were performed by an operator blinded to the experimental conditions.

Telemetric ECG

ECG recordings were acquired from conscious, freely mobile animals using a Dataquest ART telemetry system (DSI)[19, 28]. All recordings were obtained at the same time of day (evening) for 6 hours (3 hours in the light, 3 hours in the dark) during a period in which the animals' quarters were undisturbed. Recordings were obtained from cryoinjured recipients of hESC-CMs, non-CMs or PSC-only on days 1, 6 and 9 post-injury and days 1, 3, 7, 10, 14, 17, 21, 24, 27 post-transplantation. All ECG traces were evaluated manually by a blinded cardiologist, who determined the total number and frequency of events including single and multiform PVCs, as well as non-sustained and sustained VT. In accordance with Lambeth convention guidelines[29], VT was defined as a run of four or more PVCs, and sustained VT as a fast ventricular rhythm of >15 beats.

Programmed electrical stimulation (PES)

PES studies were performed on day +28 post-transplantation, using methods modified from Gutstein et al[30]. In brief, each animal was mechanically ventilated, anesthetized with 2% isoflurane, and outfitted for standard surface ECG recordings (ADInstruments). A midline incision was made in the epigastric region, and a custom-designed bipolar stimulating electrode (FHC) was inserted through the diaphragm into direct contact with the cardiac apex. PES studies were then performed using an isolated stimulator-generator (STG-1000,

MultiChannel Systems) with the pulse output set at twice the capture threshold and the pulse width at 1 millisecond (ms). We employed standard clinical PES protocols, including the application of single, double and triple extra-stimuli after a train of eight conditioning stimuli at a 150 ms cycle length. To determine the ventricular effective refractory period (VERP), a first extra-stimulus (S2) was applied with the S1–S2 interval decreased in 5 ms increments from 150 ms until the occurrence of loss of capture. The heart was then challenged three times with the train of eight followed by the single extra-stimulus (with the S1–S2 interval set at VERP+10ms). If no VT was induced, this procedure was repeated to apply three challenges with double and, if necessary, triple extra-stimuli. In each case, the coupling interval between the final two pulses was set at the VERP for the last extra-stimulus + 10ms. VT was only induced in cryoinjured animals with the application of a triple extra-stimulus. Of note, VT induction by PES was strongly associated with a history of spontaneous VT during the final day of telemetry monitoring ($p<0.001$ by McNemar's test).

Generation of the GCaMP reporter hESC line

A transgene encoding for the constitutive expression of GCaMP3 was inserted into the AAVS1 locus in H7 hESCs, using methods adapted from by Hockemeyer et al[21] (see Fig. 3a–b). In brief, the right and left arms of an AAVS1-specific ZFN were de novo synthesized (Genscript) and cloned into a single polycistronic plasmid in which the expression of each was driven by an independent human PGK promoter. A second polycistronic vector was generated in which ~800 bp homology arms flanking the AAVS1 ZFN cut site (pZDonor, Sigma Aldrich) surrounded a 5.1 kb insert with two elements: a cassette in which the CAG promoter drives expression of GCaMP3[5] (Addgene, plasmid #22692) and a second cassette encoding for PGK-driven expression of neomycin resistance.

AAVS1 ZFN (5 ug) and AAVS1 CAG GCaMP3 targeting vector (40 ug) plasmids were co-electroporated (Lonza, Nucleofection system) into H7 hESCs cultured in MEF-CM supplemented with 10 μM Y-27632. Green fluorescent colonies were isolated and expanded and selected with 40–100 μg/mL G418 (Invitrogen) for 5–10 days. GCaMP3 H7 hESCs showed a normal karyotype.

Southern Blot

Wild-type and transgenic GCaMP3+ hESC genomic DNA were digested with the restriction enzyme SphI, run on 1% polyacrylamide gel and transferred to a membrane (BioRad Zeta Probe). The membrane was washed in 2x SSC and dried at 80°C in a hybridization oven for 2 hours, followed by 1 hour of pre-hybridization in 50% formamide, 0.12 M NaH_2PO_4, 0.25 M NaCl, 7% SDS, and 1 mM EDTA at 43°C. A hybridization probe was generated with the following primers: CCTGTTAGGCAGATTCCTTATC (sense), AGATGGTGGACGAGGAAGGGG (antisense). The probe was labeled with ^{32}P dCTP (Amersham Megaprime DNA labeling system) and hybridized overnight in hybridization buffer at 43°C. After 24 hours, the membrane was washed for 20 minutes with 2x SSC/0.1% SDS followed by 20 minutes in 0.1x SSC/0.1% SDS. The membrane was then exposed to autoradiographic film for 3 days. The wildtype band is expected at 6.5 kb, while the targeted locus shifts to 2.9 kb.

Imaging of GCaMP3-expresssing grafts

Intravital imaging of hearts with GCaMP3+ grafts was performed on days 14 and 28 post-transplantation using either an open-chest or ex vivo preparation. For the open-chest preparation, guinea pigs were anesthetized, mechanically ventilated, and outfitted for standard surface ECG recordings, as described above. The anterior epicardium was then exposed by a wide thoracotomy and visualized using an epifluorescence stereomicroscope (Nikon, SMZ 1000) equipped with an EXFO X-Cite illumination source. GCaMP3 was excited at 450–490 nm and bandpass filtered (500–550 nm) prior to detection by an electron-multiplying, charge-coupled device camera (Andor iXon 860 EM-CCD) controlled by Andor Solis software. GCaMP3 image acquisition was typically at 80–140 fps. Signals from the CCD camera and the surface ECG were fed through a computer for digital storage and off-line analysis using Andor software and custom Matlab scripts (MathWorks).

Some engrafted hearts were also imaged ex vivo after mechanical arrest to eliminate motion artifacts. For these experiments, the heart was harvested, rapidly mounted on a gravity-fed Langendorff apparatus and then perfused with modified Tyrode solution at 37 C. The epicardial GCaMP3 signal was then recorded before and after supplementation of the perfusate with an excitation-contraction uncoupler, either 2,3-butanedione monoxime (BDM, 20 mM)[31, 32] or blebbistatin (10 μM)[33]. The utility of blebbistatin was limited by its significant blue-green fluorescence[34], which somewhat interfered with the acquisition of the GCaMP3 signal, so BDM was used in experiments except where otherwise indicated (see Supplementary Table S3). All quantitative comparisons were performed using hearts treated with the same uncoupler. The electrical activity of the isolated heart was continuously monitored by placing positive and negative ECG leads at the base of the right ventricle and left ventricular apex, respectively. Although most imaging experiments were performed under spontaneous conditions, a subset of hearts was also imaged during external pacing at rates from 3–6 Hz (ML866 PowerLab 430 Data Acquisition System). Experiments involving pacing at rates >5 Hz were sometimes limited by the occurrence of lethal tachyarrhythmias.

In a subset of hearts, GCaMP3 activation maps were generated by determining the interval between a pacing stimulus (or the host QRS complex) and the initial rise in GCaMP3 fluorescence. For this analysis, raw data from the green fluorescence and ECG channels were read into a custom Matlab script for analysis. The GCaMP3 fluorescent signal was median-filtered in time to reduce noise, smoothed with a spatial conical filter, and background subtracted. Regions of graft were user-defined and then analyzed to determine the relative GCaMP3 activation time on a per-pixel basis. Relative GCaMP3 activation times for each pixel were then averaged over several stimuli to generate GCaMP3 activation maps.

Voltage mapping studies

The preceding imaging system and experimental preparation was also used in optical mapping studies with the potentiometric dye RH237. RH237 was selected as our dye of choice, given our past published experience with this indicator and its reasonable spectral separation from GCaMP3. When examined in the same heart, GCaMP3 (green channel) and

RH237 (red channel) fluorescent signals were acquired consecutively by an exchange of filter cubes, not simultaneously.

In brief, cryoinjured hearts with or without 28-day old GCaMP3+ hESC-CM grafts were mounted on a Langendorff apparatus and loaded with RH237 (40 μM) by a bolus injection (in 10 mL buffer) into the aorta. After an initial stabilization period, RH237-stained hearts were then imaged during both spontaneous and paced rhythms. RH237 was excited at 520–550 nm, while emitted light was long-pass filtered (670 nm) prior to detection at 500 fps by the aforementioned high-speed EM-CCD system. The resultant fluorescent signals were analyzed as previously described[35–37]. In brief, background fluorescence was subtracted and the signal at each pixel was smoothed using a median temporal filter and a spatial cone filter. The signal at each pixel was then scaled as a percentage of the maximum optical action potential amplitude for all the pixels. While not simultaneously acquired, RH237 and GCaMP3 signals could be partially correlated in a subset of paced hearts by aligning repetitive signals relative to the stimulating electrode.

Histology

Histological studies were performed as previously detailed by our group[2, 38, 39]. For immunohistochemistry, we used the primary antibodies detailed in Supplementary Table 4, followed by either fluorescent secondary antibodies (Alexa-conjugated, species-specific antibodies from Molecular Probes) or the avidin-biotin reaction followed by chromogenic detection (ABC kits from Vector Labs). The guinea pig-specific in situ hybridization probe was generated using methods adapted from Kuznetsov et al[40]. In brief, guinea pig genomic DNA was amplified using PCR primers reported by the aforementioned authors (sense: 5′-CTCCTGTCCTGCATCCACT-3′; antisense: 5′-GGATATGAGAGACAGTGGTG-3′). The resultant 345-bp band was excised and then amplified in a second round of PCR doped with digoxigenin-11-dUTP. Subsequent in situ hybridization with this digoxigenin-labeled guinea pig-specific probe was performed using methods previously detailed for the human-specific pan-centromeric probe.[1] For detection, we used a peroxidase-conjugated anti-digoxigenin antibody (Roche), followed by staining with either a chromogenic substrate or fluorescent tyramide signal amplification kit (Molecular Probes).

Statistical analysis

All data were analyzed in a blinded manner, with the breaking of the identifier code only after the analysis was completed. All values were expressed as mean ± standard error. Statistical analyses were performed using PASW Statistics 18, Graphpad Prism and SAS software, with the threshold for significance set at level $p < 0.05$. Echocardiographic outcomes were analyzed by ANOVA followed by post-hoc comparisons between groups by Tukey HSD and time-course changes by paired t-test analysis of means. For comparisons of the fraction of animals showing spontaneous or induced arrhythmias, we employed a two-sided Fisher's exact test. For comparisons involving the semi-quantitative PES arrhythmia score, a non-parametric parameter, we used the Kruskal–Wallis test followed by post-hoc Mann-Whitney U-testing. The incidence of spontaneous arrhythmias was analyzed using a Poisson regression model to adjust for repeated measures and the effect of time. This approach was used to calculate the ratio of the observed frequencies of recurrence for the

two groups and the 95% confidence interval. We used the McNemar's test for correlated proportions to test for an association between induced VT by and spontaneous VT either on the final day of monitoring or throughout the day 3–28 post-transplantation monitoring period. To test for synchrony between GCaMP3 fluorescence and ECG signals, intervals were compared by ANOVA followed by post-hoc Dunnett's test.

Supplementary Material

Refer to Web version on PubMed Central for supplementary material.

Acknowledgments

We thank Dr. Yvonne Tallini, Luz Linares, Brian Johnson and Sarah Dupras for advice and technical assistance. This work was supported in part by a grant from Geron Corporation (MAL), as well as by NIH grants K08-HL80431 (MAL), R01-HL064387 (MAL and CEM), P01-HL094374 (MAL and CEM), R01-HL084642 (CEM), P01-GM81619 (CEM), U01-HL100405 (MAL and CEM) and R01-HL095828 (NS and MWK). Animal experiments were supported in part by the UW's Mouse Metabolic Phenotyping Center, U24-DK076126.

References

1. Caspi O, et al. Transplantation of human embryonic stem cell-derived cardiomyocytes improves myocardial performance in infarcted rat hearts. J Am Coll Cardiol. 2007; 50:1884–1893. [PubMed: 17980256]
2. Laflamme MA, et al. Cardiomyocytes derived from human embryonic stem cells in pro-survival factors enhance function of infarcted rat hearts. Nat Biotechnol. 2007; 25:1015–1024. [PubMed: 17721512]
3. van Laake LW, et al. Human embryonic stem cell-derived cardiomyocytes survive and mature in the mouse heart and transiently improve function after myocardial infarction. Stem Cell Research. 2007; 1:9–24. [PubMed: 19383383]
4. Tallini YN, et al. Imaging cellular signals in the heart in vivo: Cardiac expression of the high-signal Ca2+ indicator GCaMP2. Proc Natl Acad Sci U S A. 2006; 103:4753–4758. [PubMed: 16537386]
5. Tian L, et al. Imaging neural activity in worms, flies and mice with improved GCaMP calcium indicators. Nature Methods. 2009; 6:875–881. [PubMed: 19898485]
6. Kehat I, et al. Electromechanical integration of cardiomyocytes derived from human embryonic stem cells. Nat Biotechnol. 2004; 22:1282–1289. [PubMed: 15448703]
7. Xue T, et al. Functional integration of electrically active cardiac derivatives from genetically engineered human embryonic stem cells with quiescent recipient ventricular cardiomyocytes: insights into the development of cell-based pacemakers. Circulation. 2005; 111:11–20. [PubMed: 15611367]
8. Gepstein L, et al. In vivo assessment of the electrophysiological integration and arrhythmogenic risk of myocardial cell transplantation strategies. Stem Cells. 2010; 28:2151–2161. [PubMed: 20960511]
9. Liao SY, et al. Proarrhythmic risk of embryonic stem cell-derived cardiomyocyte transplantation in infarcted myocardium. Heart Rhythm. 2010; 7:1852–1859. [PubMed: 20833268]
10. Roell W, et al. Engraftment of connexin 43-expressing cells prevents post-infarct arrhythmia. Nature. 2007; 450:819–824. [PubMed: 18064002]
11. Kehat I, et al. Human embryonic stem cells can differentiate into myocytes with structural and functional properties of cardiomyocytes. J Clin Invest. 2001; 108:407–414. [PubMed: 11489934]
12. He JQ, Ma Y, Lee Y, Thomson JA, Kamp TJ. Human embryonic stem cells develop into multiple types of cardiac myocytes: action potential characterization. Circ Res. 2003; 93:32–39. [PubMed: 12791707]
13. Zhu WZ, et al. Neuregulin/ErbB signaling regulates cardiac subtype specification in differentiating human embryonic stem cells. Circ Res. 2010; 107:776–786. [PubMed: 20671236]

14. Mandel Y, et al. Human embryonic and induced pluripotent stem cell-derived cardiomyocytes exhibit beat rate variability and power-law behavior. Circulation. 2012; 125:883–893. [PubMed: 22261196]
15. Jonsson MK, et al. Quantified proarrhythmic potential of selected human embryonic stem cell-derived cardiomyocytes. Stem Cell Research. 2010; 4:189–200. [PubMed: 20303332]
16. Chen HS, Kim C, Mercola M. Electrophysiological challenges of cell-based myocardial repair. Circulation. 2009; 120:2496–2508. [PubMed: 20008740]
17. Swoap SJ, Overton JM, Garber G. Effect of ambient temperature on cardiovascular parameters in rats and mice: a comparative approach. Am J Physiol Regul Integr Comp Physiol. 2004; 287:R391–396. [PubMed: 15087284]
18. Mummery C, et al. Differentiation of human embryonic stem cells to cardiomyocytes: role of coculture with visceral endoderm-like cells. Circulation. 2003; 107:2733–2740. [PubMed: 12742992]
19. Shiotani M, Harada T, Abe J, Hamada Y, Horii I. Methodological validation of an existing telemetry system for QT evaluation in conscious guinea pigs. J Pharmacol Toxicol Methods. 2007; 55:27–34. [PubMed: 16831559]
20. Zhu WZ, Van Biber B, Laflamme MA. Methods for the derivation and use of cardiomyocytes from human pluripotent stem cells. Methods Mol Biol. 2011; 767:419–431. [PubMed: 21822893]
21. Hockemeyer D, et al. Efficient targeting of expressed and silent genes in human ESCs and iPSCs using zinc-finger nucleases. Nature Biotechnology. 2009; 27:851–857.
22. Lieu DK, et al. Absence of transverse tubules contributes to non-uniform Ca(2+) wavefronts in mouse and human embryonic stem cell-derived cardiomyocytes. Stem Cells and Development. 2009; 18:1493–1500. [PubMed: 19290776]
23. Kotlikoff MI. Genetically encoded Ca2+ indicators: using genetics and molecular design to understand complex physiology. J Physiol. 2007; 578:55–67. [PubMed: 17038427]
24. Thomson JA, et al. Embryonic stem cell lines derived from human blastocysts. Science. 1998; 282:1145–1147. [PubMed: 9804556]
25. Xu C, et al. Feeder-free growth of undifferentiated human embryonic stem cells. Nat Biotechnol. 2001; 19:971–974. [PubMed: 11581665]
26. Li Y, Powell S, Brunette E, Lebkowski J, Mandalam R. Expansion of human embryonic stem cells in defined serum-free medium devoid of animal-derived products. Biotechnol Bioeng. 2005; 91:688–698. [PubMed: 15971228]
27. Xu C, et al. Efficient generation and cryopreservation of cardiomyocytes derived from human embryonic stem cells. Regenerative Medicine. 2011; 6:53–66. [PubMed: 21175287]
28. Shiotani M, et al. Practical application of guinea pig telemetry system for QT evaluation. J Toxicol Sci. 2005; 30:239–247. [PubMed: 16141657]
29. Walker MJ, et al. The Lambeth Conventions: guidelines for the study of arrhythmias in ischaemia infarction, and reperfusion. Cardiovasc Res. 1988; 22:447–455. [PubMed: 3252968]
30. Gutstein DE, Danik SB, Sereysky JB, Morley GE, Fishman GI. Subdiaphragmatic murine electrophysiological studies: sequential determination of ventricular refractoriness and arrhythmia induction. Am J Physiol Heart Circ Physiol. 2003; 285:H1091–1096. [PubMed: 12750061]
31. Biermann M, et al. Differential effects of cytochalasin D and 2,3 butanedione monoxime on isometric twitch force and transmembrane action potential in isolated ventricular muscle: implications for optical measurements of cardiac repolarization. J Cardiovasc Electr. 1998; 9:1348–1357.
32. Laurita KR, Singal A. Mapping action potentials and calcium transients simultaneously from the intact heart. Am J Physiol Heart Circ Physiol. 2001; 280:H2053–2060. [PubMed: 11299206]
33. Fedorov VV, et al. Application of blebbistatin as an excitation-contraction uncoupler for electrophysiologic study of rat and rabbit hearts. Heart Rhythm. 2007; 4:619–626. [PubMed: 17467631]
34. Kolega J. Phototoxicity and photoinactivation of blebbistatin in UV and visible light. Biochem Biophys Res Commun. 2004; 320:1020–1025. [PubMed: 15240150]

35. Asfour H, Swift LM, Sarvazyan N, Doroslovacki M, Kay MW. Signal decomposition of transmembrane voltage-sensitive dye fluorescence using a multiresolution wavelet analysis. IEEE Trans Biomed Eng. 2011; 58:2083–2093. [PubMed: 21511560]

36. Kay M, Swift L, Martell B, Arutunyan A, Sarvazyan N. Locations of ectopic beats coincide with spatial gradients of NADH in a regional model of low-flow reperfusion. Am J Physiol Heart Circ Physiol. 2008; 294:H2400–2405. [PubMed: 18310518]

37. Swift L, et al. Controlled regional hypoperfusion in Langendorff heart preparations. Physiol Meas. 2008; 29:269–279. [PubMed: 18256457]

38. Fernandes S, et al. Human embryonic stem cell-derived cardiomyocytes engraft but do not alter cardiac remodeling after chronic infarction in rats. J Mol Cell Cardiol. 2010; 49:941–949. [PubMed: 20854826]

39. Laflamme MA, et al. Formation of human myocardium in the rat heart from human embryonic stem cells. Am J Pathol. 2005; 167:663–671. [PubMed: 16127147]

40. Kuznetsov SA, et al. Circulating skeletal stem cells. J Cell Biol. 2001; 153:1133–1140. [PubMed: 11381097]

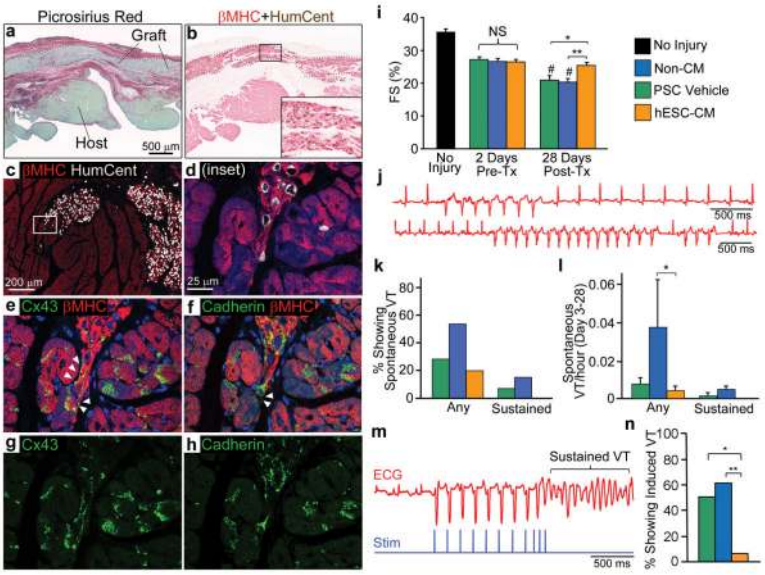

Figure 1. Transplanted hESC-CMs partially remuscularize injured guinea pig hearts, preserve mechanical function, and reduce arrhythmia susceptibility

a–b, 28 day-old hESC-CM grafts in a cryoinjured heart stained with picrosirius red (a) and anti-β-myosin heavy chain (βMHC, red) plus human-specific in situ probe (HumCent, brown) (**b**). **c–d,** Confocal image of host-graft contact dual-labeled for HumCent (white) and βMHC (red), destained and then immunostained for βMHC (red) and either connexin-43 (**e&g**, Cx43, green) or cadherins (**f&h**, green). Arrows indicate Cx43 and cadherin shared between graft and host myocytes. **i,** LV fractional shortening (FS) by echocardiography in uninjured animals and cryoinjured recipients of PSC vehicle-only, non-CMs or hESC-CMs. **j,** Representative telemetric ECGs, including non-sustained VT in a hESC-CM recipient (upper), as well as sustained VT and triplet PVCs in a non-CM recipient (lower). **k,** Percentage of animals by group that showed spontaneous VT during monitoring from days 3–28 post-transplantation. **l,** Frequency of spontaneous VT by group. **m,** ECG (red) and stimulation (blue) traces from a cryoinjured non-CM recipient induced to sustained VT by PES. **n,** Percentage of animals in each group induced to VT. All data are presented as mean ± SEM; n ≥13 per group. NS, no significant difference. *, $p<0.05$ between groups. **, $p<0.01$ between groups.#, $p<0.05$ versus day −2.

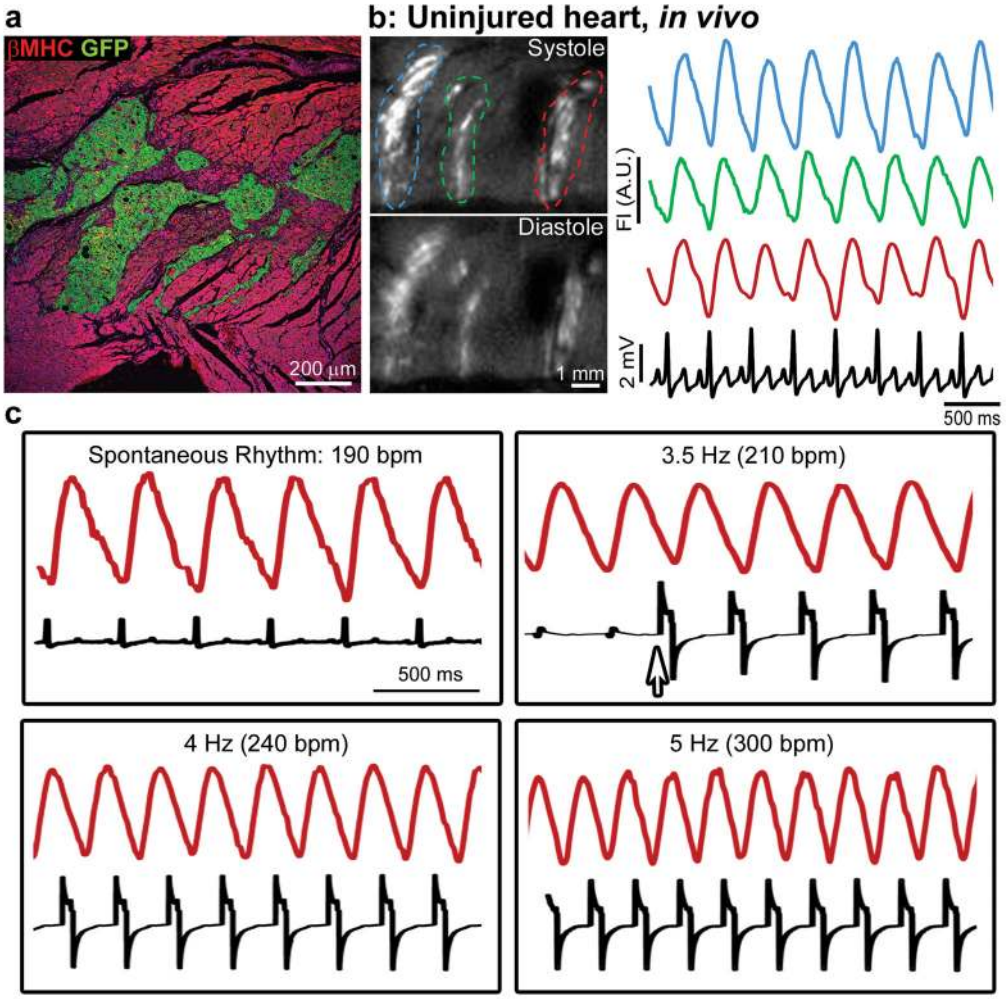

Figure 2. hESC-CM grafts in uninjured hearts show 1:1 coupling with host myocardium

a, GCaMP3+ hESC-CM graft in an uninjured heart immunostained for GFP (green) and βMHC (red), showing extensive host-graft contact with minimal intervening scar. **b,** Left: GCaMP3+ hESC-CM graft in an uninjured heart during systole and diastole, acquired using an open-chest preparation at 14-days post-transplantation. Right: GCaMP3 fluorescence intensity versus time for the red, green and blue regions of interest, as well as the host ECG (black). GCaMP3 fluorescent transients in all three regions occurred in a 1:1 correspondence with QRS complexes of the host ECG. **c,** GCaMP3 fluorescent signal (red) and ECG (black) from a representative hESC-CM graft in an uninjured heart, imaged ex vivo under mechanical arrest. 1:1 host-graft coupling occurred during spontaneous beating and pacing at rates ≤5 Hz. Arrow = onset of pacing.

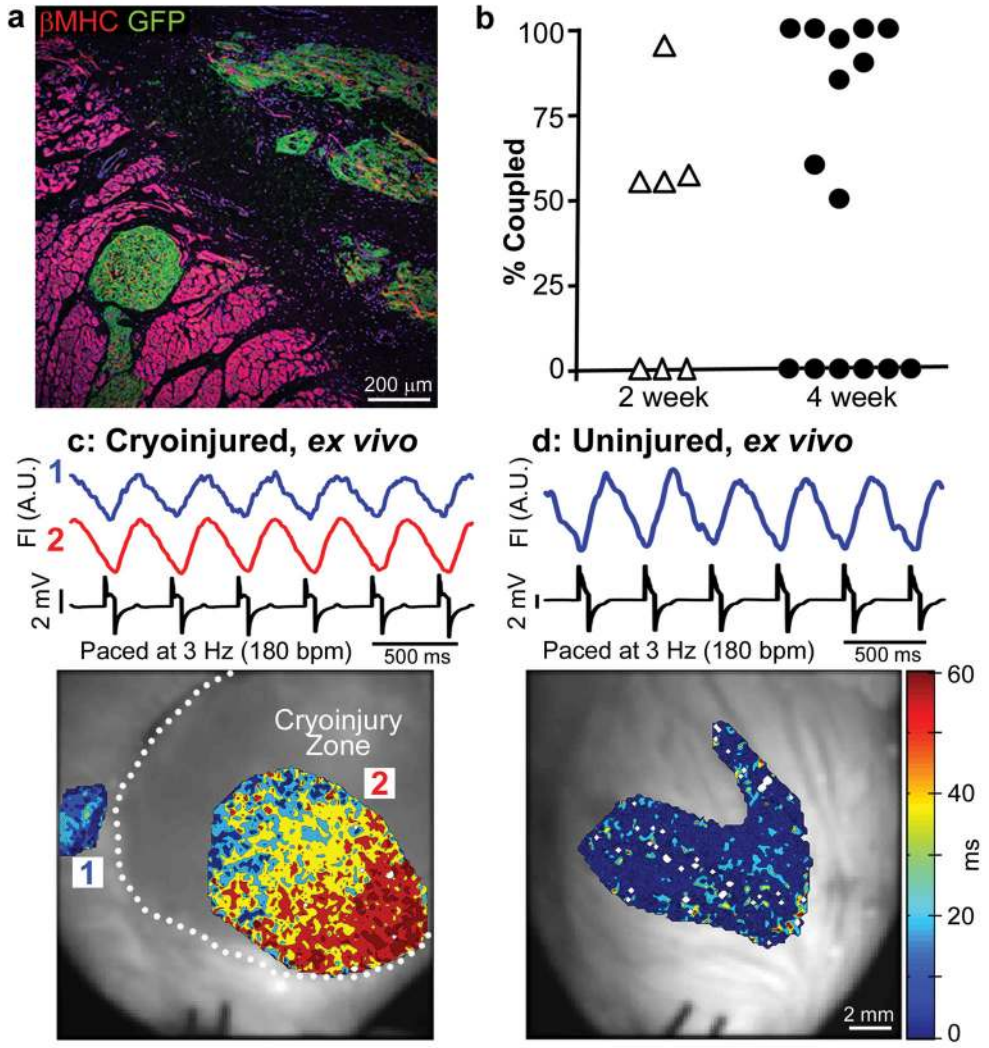

Figure 3. hESC-CM grafts show 1:1 host-graft coupling in a majority of injured recipient hearts, but the extent of coupling and pattern of activation is more variable

a, GCaMP3+ hESC-CM graft in a cryoinjured heart immunostained for GFP (green) and βMHC (red). Small graft nests were located in host muscle within the border zone, but most of the graft was in scar. **b,** Percentage of visible GCaMP3+ hESC-CM graft in each cryoinjured heart that showed 1:1 host-graft coupling at 14- and 28-days post-transplantation (n=7 and n=15 animals, respectively). **c,** Representative 28-day-old GCaMP3+ hESC-CM graft in a cryoinjured heart imaged ex vivo during mechanical arrest with blebbistatin and pacing at 3 Hz. Upper: Traces of mean fluorescent intensity versus time for graft regions located within host muscle (‘1’, blue) and the cryoinjury zone (‘2’, red). Both were activated in a 1:1 correlation with the host ECG (black). Lower: Corresponding activation map showing the interval (in ms) between the stimulus pulse and the local rise in GCaMP3 fluorescence. Graft in host muscle (1) showed uniformly rapid activation, while graft in scar (2) activated first in central scar and then gradually progressed toward the border zone. In other instances, graft activation started at the border zone and radiated into the scar. **d**, GCaMP3 fluorescence and EGG traces (upper) as well as the activation map (lower) for a

representative GCaMP3+ hESC-CM graft in a blebbistatin-arrested uninjured heart. This graft showed 1:1 host-graft coupling and a brief interval between stimulus and GCaMP3 transient upstroke.